PNAS
www.pnas.org

## Supplementary Information for

# A second S4 movement opens hyperpolarization-activated HCN channels

Xiaoan Wu, Rosamary Ramentol, Marta E Perez, Sergei Yu Noskov, H Peter Larsson

H Peter Larsson
Email: PLarsson@med.miami.edu

**This PDF file includes:**

Figures S1 to S9
Tables S1 to S2
Legend for Movie S1
Legend for Datasets S1
SI References

**Other supplementary materials for this manuscript include the following:**

Movie S1
Datasets S1

**Supplementary Figures**

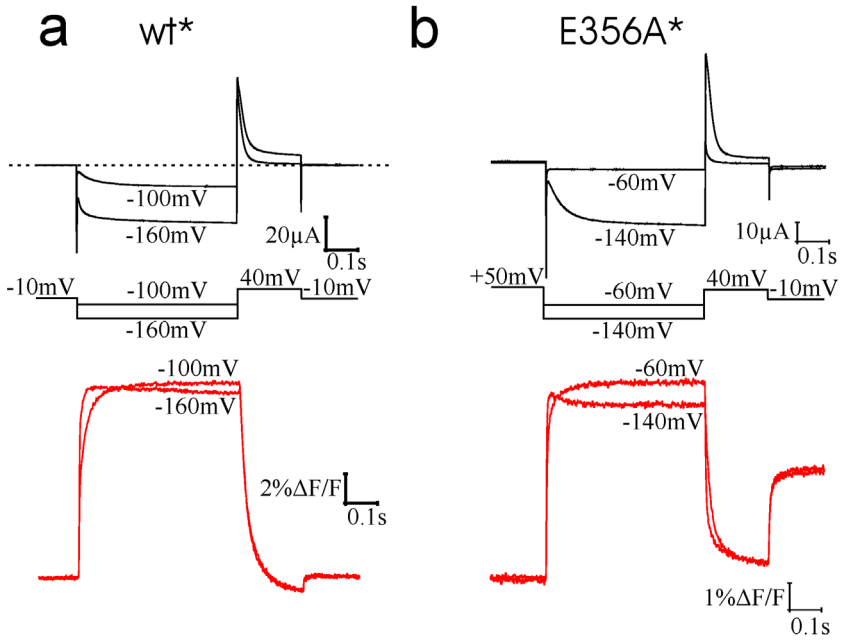


**Suppl. Figure. S1. Similar fluorescence in wt* and E356A* suggest similar S4 movements.** a-b) Currents (top) and fluorescence (bottom) from a) wt* and b) E356A* channels in response to the indicated voltage steps (middle).

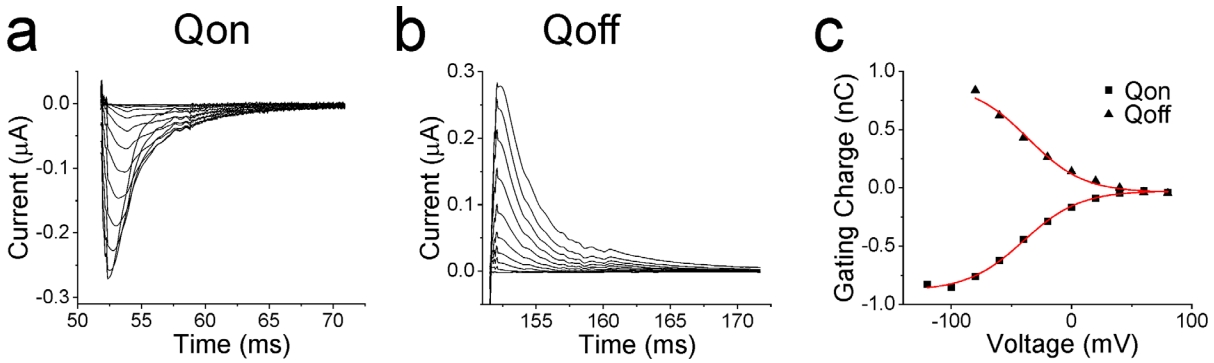


**Suppl. Fig. S2. Gating currents from R332C/E356A/P435Y channels. a)** On gating currents in response to voltage steps between +60mV and -140mV from a pre-pulse of +80 mV. **b)** Off gating currents in response to a voltage step to +80 mV after voltage steps between +60mV and -100 mV. Off gating currents only shown for voltage steps less negative than -100 mV due to endogenous currents developing over time in response to voltages more negative than -100 mV. **c)** On and Off QV curves generated by integrating the currents in a and b from a representative oocyte. Data fit by Boltzmann curves with parameters: On: $V_{1/2}$ = -39.9 mV, z =1.09 $e_0$, A = 0.9 nC. Off: $V_{1/2}$ = -36.3 mV, z =1.09 (fixed) $e_0$, A = 0.92 nC. z was held fixed between the two fits due to the lack of saturation in the Qoff. Note the similar amplitude of the Qon and Qoff from the same oocyte.

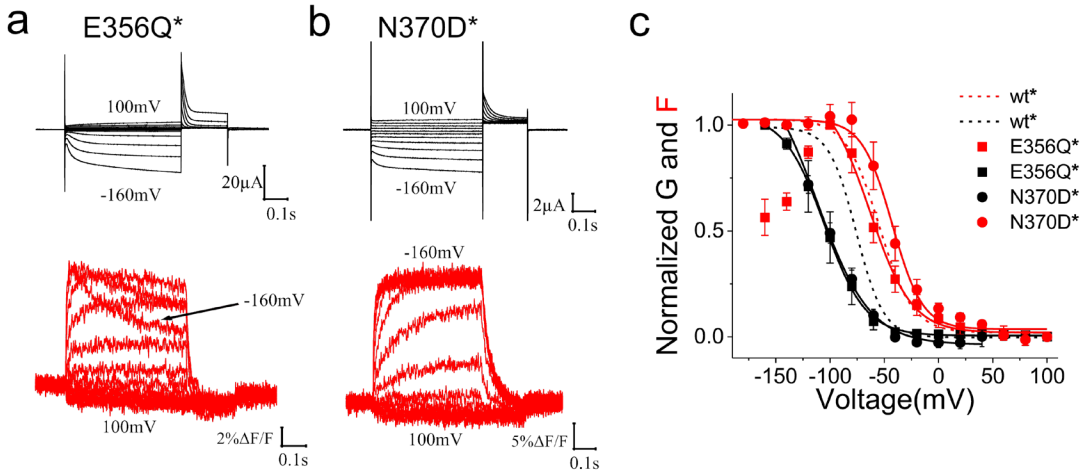


**Suppl. Fig S3. Channels with hydrogen-bonding residues at E356 and N370 gate normally.** Representative traces of the current (black) and fluorescence (red) from **a)** E356Q* and **b)** N370D* channels. **c)** Normalized G(V) and F(V) curves of wt*, E356Q*, and N370D* channels. Mean ± SEM.

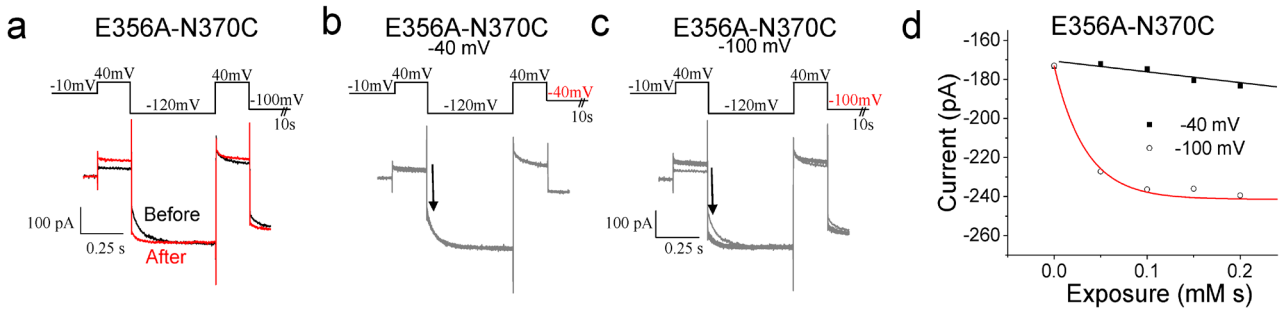


**Suppl. Fig. S4**. **a)** Currents before (black) and after (red) application of 10 μM MTSET for 100 s to the cytosolic side of E356A-N370C channels while voltage clamped at -100 mV. (top) Voltage protocol. **b-c)** Currents during the application of MTSET to E356A-N370C channels held mainly (10 s out of 11.5 s) at **b)** -40 mV or **c)** -100 mV. Currents from **b)** and **c)** were measured from the same patch. (top) Voltage protocol. The step at the end of the protocol lasted 10 s. **d)** Currents measured at the arrow in **b)** and **c)** from E356A-N370C channels during MTSET application at -40 mV (closed squares) and -100 mV (open circles: fitted with an exponential function). The average modification rates of E356A-N370C was 25,460 ± 9,758 $M^{-1}s^{-1}$ (n = 3) at -100 mV and decreased to 1,968 ± 731 $M^{-1}s^{-1}$ (n= 3) at -40 mV.

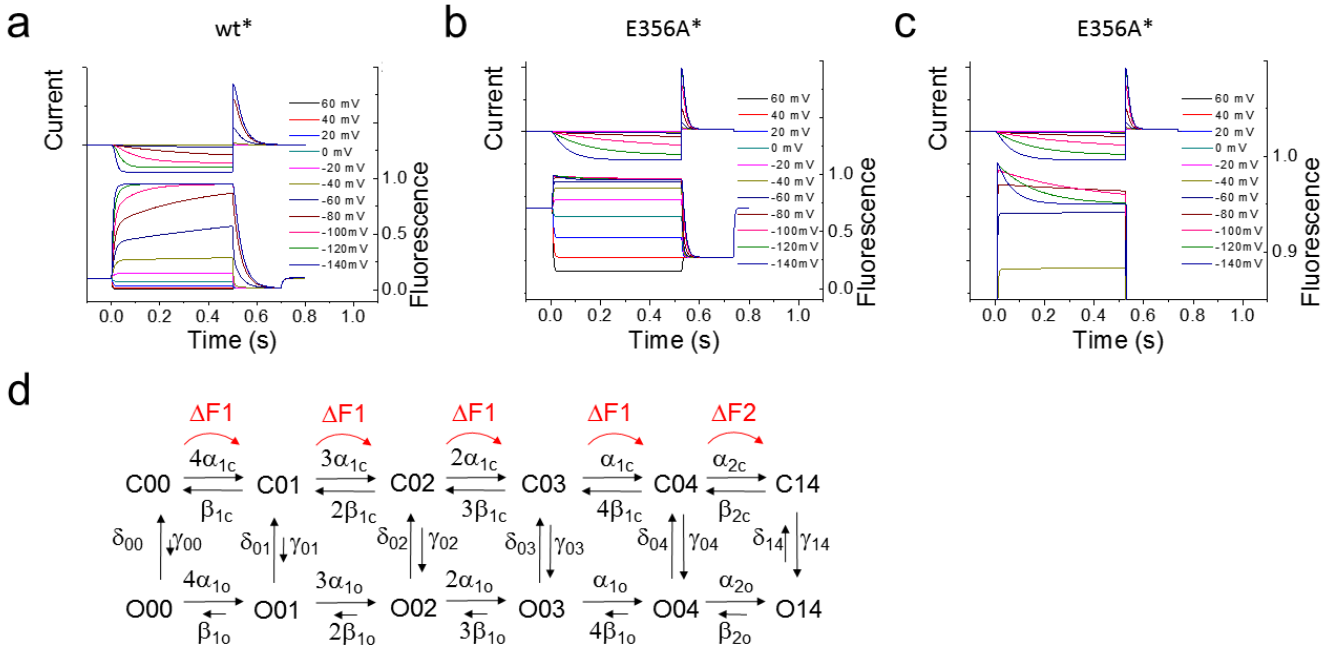


**Suppl. Figure S5. Two-step S4 movement model reproduces wt* and E356A* fluorescence and currents.**

**a-b)** Current (top) and fluorescence (bottom) from the **a)** wt* and **b)** E356A* spHCN channel models in response to voltage steps from +60 mV to -140 mV (ΔV = 20 mV) from a holding voltage of -10 mV and with a $V_{tail}$ = +40 mV. See Suppl. Fig. S6 for a comparison of model and data. **c)** Fluorescence from the E356A* channel model in response to voltage steps from -40 mV to -140 mV at higher magnification to better show the correlation of the second fluorescence component with the current kinetics and voltage dependence. **d)** 2-step S4 movement model. The horizontal steps are S4 moving in two voltage-dependent steps – the first step is independent in the four subunits, the second one is cooperative in all four subunits – generating two different type of fluorescence changes (an increase ΔF1 and a decrease ΔF2). The S4 on-rates between closed states are $\alpha_{ic} = k_i \exp(-z_i(V-V_{1/2}(i))/kT)$ and off-rates $\beta_{ic} = k_i \exp(+z_i(V-V_{1/2}(i))/kT)$ for i = 1 and 2 for the first and second S4 steps, respectively. Horizontal steps in the open states are set by micro-reversibility, i.e. $\alpha_{io} = \alpha_{ic} L_i$ and $\beta_{io} = \beta_{io}/L_i$. Vertical steps are voltage-independent opening-closing conformational changes, with opening rates $\gamma_{0n} = \gamma_{00} L_i^n$ and closing rates $\delta_{0n} = \delta_{00}/L_i^n$, for n = 0, 1, 2, 3, and 4 (where n stands for the number of subunits that have undergone the first S4 step) and final opening rates $\gamma_{14} = \gamma_{04} L_2$ and closing rates $\delta_{14} = \delta_{04}/L_2$. The first S4 step, we assume occurs independently in the four subunits and generates a large increase in fluorescence (ΔF1), whereas we assume that the second S4 step occurs in a concerted fashion in all four subunits and generates a small decrease in fluorescence (ΔF2). Each step in S4 increases the open probability. The main difference in the wt* and E356A* models is changes in the $V_{1/2}$ of the S4 steps (see Suppl. Table S2). See Supplementary Table S2 for parameters.

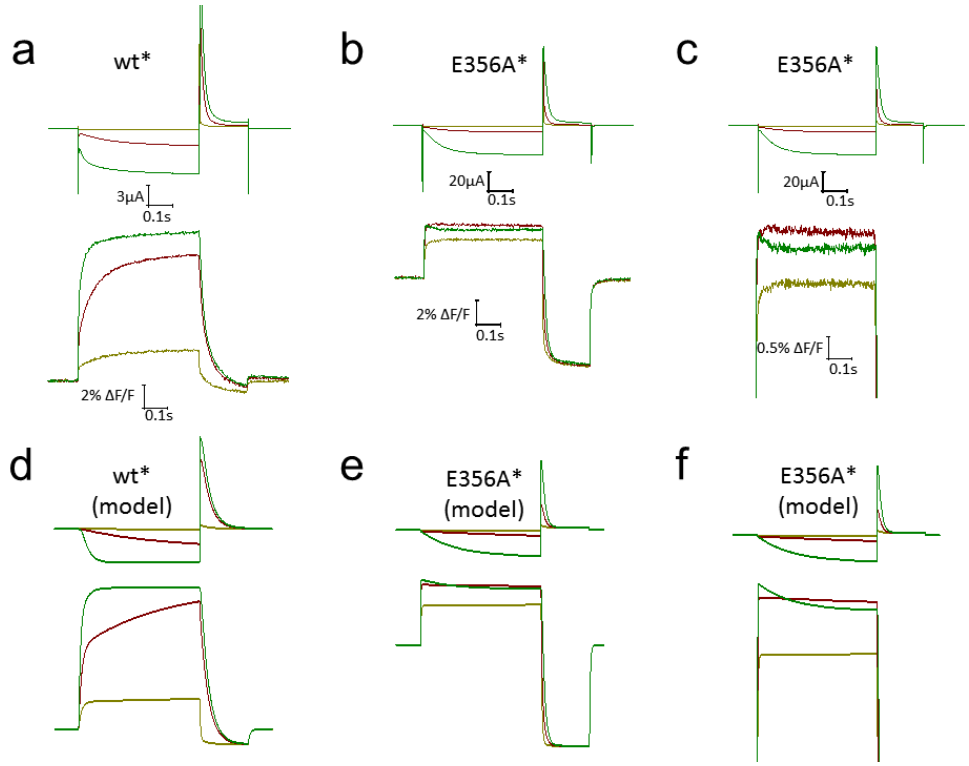


**Suppl. Figure S6. Detail comparison of the fluorescence and currents from the model and wt* and E356A* fluorescence and currents.**

Current (top) and fluorescence (bottom) from: **a)** wt*, **b)** E356A*, and **c)** E356A* with fluorescence at higher magnification, **d)** Model of wt*, **e)** Model of E356A*, and **f)** Model of E356A* (with fluorescence at higher magnification) spHCN channels in response to three voltage steps to -40 mV, -80 mV, and -120 mV from a holding voltage of -10 mV and with a $V_{tail}$ = +40 mV. **a and d)** In wt* channels, a voltage step to -40 mV generates a fast fluorescence change followed by an equally large slow fluorescence change. Few channels open at -40 mV. We interpret the fast fluorescence as the first (C00 through C04) transitions in a subset of channels. The slow increasing fluorescence change, we interpret as due to that some of these channels undergoing the slower second (C04 to C14) transition, which seemingly paradoxically leads to an increase in fluorescence. This is due to, as in any Markov-chain model, that if some channels undergo the second transition then other channels will, on average, re-establish the equilibrium between the number of channels in the C00 and C04 states. This will lead to, on average and with time, that additional channels will have undergone the first (C00 through C04) transitions. Because the first transition leads to a large increase in fluorescence compared to the smaller decrease in fluorescence for the second transition, this is the reason for the slow increase in fluorescence. During the tail voltage at +40 mV after the -40 mV step, around half of the fluorescence returns quickly followed by a slow fluorescence component. The fast return of the fluorescence upon depolarization is due to the channels that did not reached C14 during the -40 mV voltage step and returning back to C00 (C04 through C00 transitions), whereas the slow return of the fluorescence is due to channels that reached C14 (or O14) during the voltage step and now slowly returning to C04 and then C00 (C14 to C04, then C04 through C00 transitions). A voltage step to -80 mV generates almost equal size fast and slow fluorescence changes. Most channels open at -80 mV. During the tail voltage at +40 mV, the fluorescence returns slowly, due

to that at -80 mV most channels have reached O14 (or at least C14) during the -80 mV step. A voltage step to -120 mV generates mainly a fast fluorescence changes, because most channels undergo the first (C00 through C04) transitions before any channels have had time to undergo the second (C04 to C14) transition. During the tail voltage at +40 mV, the fluorescence returns slowly, due to that at -120 mV all channels have reached O14 during the -120mV step. **b and e)** In E356A* channels, a voltage step to -40 mV generates mainly a fast fluorescence change of almost maximal amplitude. Few channels open at -40 mV. During the tail voltage at +40 mV, the fluorescence returns quickly. We interpret the fast fluorescence as (C00 through C04) transitions and the fast return of the fluorescence as the C04 through C00 transitions. A voltage step to -80 mV generates an only slightly larger fluorescence change than for -40 mV. However, a second slow fluorescence change is seen as a decrease in fluorescence (better seen at higher magnification in panels c and f) that correlates with channel opening kinetics. Most channels open at -80 mV. During the tail voltage at +40 mV, the fluorescence returns slower, due to that at -80 mV most channels have reached O14 (or at least C14) during the -80-mV step. A voltage step to -120 mV generates a fast fluorescence changes followed by a small decrease in the fluorescence when channels undergo the second transition. Upon depolarization, the fluorescence returns slowly, due to that most channels have reached O14 during the -120-mV step.

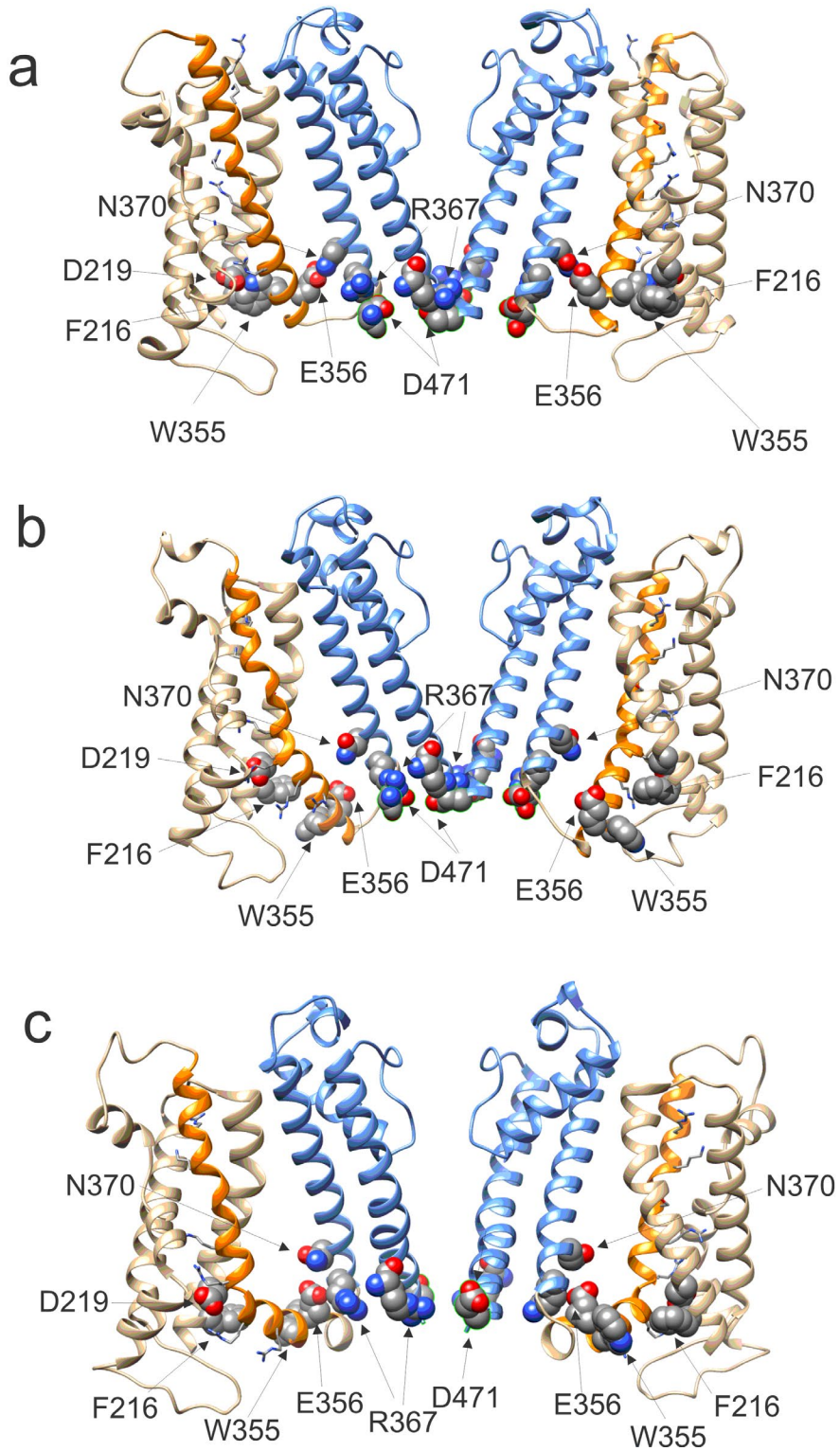


**Suppl. Fig. S7. Molecular models of S4 outward/closed, S4 intermediate/closed, and S4 inward/open state. a)** Molecular model of the spHCN channel in the closed state with S4 outward based on the cryo-EM structure of closed hHCN1 with S4 outward [1]. **b)** Molecular model of the spHCN channel in the closed state with S4 in the intermediate state based on the

cryo-EM structure of the closed hHCN1 with S4 inward [2], but the VSD was remodeled to approximate the conformation of S1-S4 as in the S4 outward state [1]. However, N-terminal part of S4 remained in the same vertical position as in the S4 inward state. The S4 helix was also straightened by rotating the C-terminal part of S4 to be more aligned with the N-terminal part of S4. The resulting conformation is similar to the closed hHCN1 structure [1] but with S4 after a two-click helical screw motion inward (See Supplementary Movie S1). **c)** Molecular model of the spHCN channel in the open state with S4 inward. The open state spHCN model with S4 inward was modelled after the cryo-EM structure of the open hERG channel [3] with the VSD replaced for the hHCN1 VSD with S4 inward [2]. The transitions between the different states are shown in Supplementary Video S1. Residues mentioned in the text and in Figure 6 are shown with space-filled side chains. S4 arginines are shown as stick. Only two diametrically-opposed subunits are shown for clarity. However, D471 and R367 are shown for all four subunits to show the intersubunit interaction between these two residues.

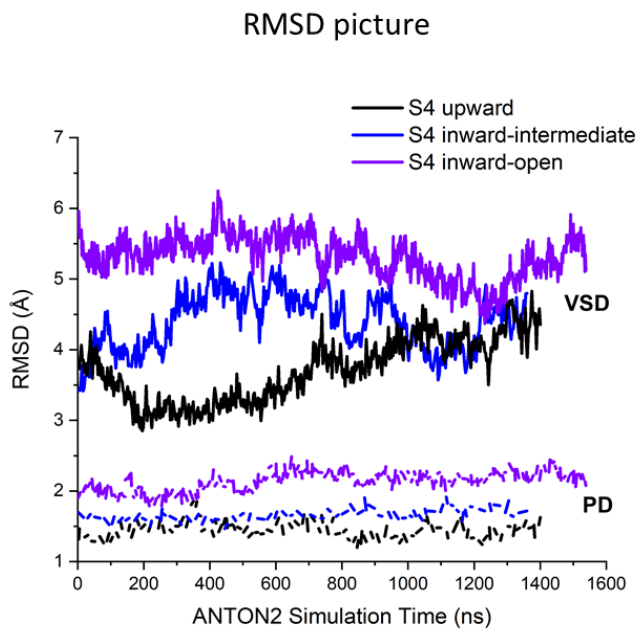


**Suppl. Figure S8. Molecular models are stable in MD simulations.** Time-traces for heavy-atom Root-Mean-Square Deviations (RMSDs) for the three conformational states studied. RMSD is evaluated relative to the starting structure with RMSD computed for Pore Domain (PD) and residues comprising Voltage-Sensing Domain (VSD) are shown as dashed and solid lines, respectively. All RMSD traces reached plateau regions and exhibit values comparable to other voltage-gated K+ channels simulated to micro-seconds time-ranges.

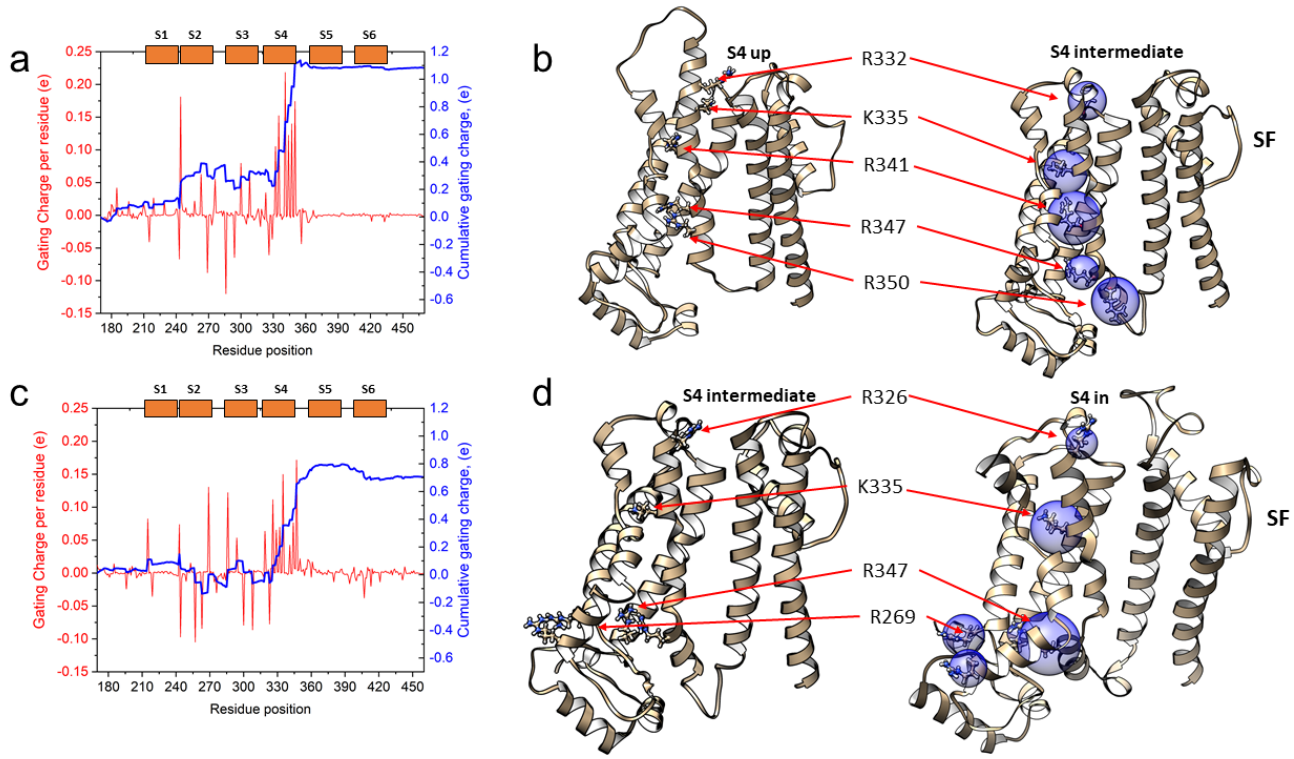


**Suppl. Figure S9. Contribution to gating charge in the two S4 steps. a)** Contributions of individual residues to the gating charge in first S4 step. (*Left* Y axis) and cumulative sums of gating charge contributions (Right Y axis and shown in a *blue line*) converge to the total gating charge of ~1.1 $e_0$ transferred for the S4 up to S4 intermediate movement (Step 1). **b)** Molecular illustration of side chains contributing more that 10 % to total gating charge movement in the first S4 step. S4 intermediate structure shows side chains contributing positively to net gating charge transfer shown with transparent blue spheres. The radius of the sphere reflects relative contribution of the residue to gating charge moved in step 1. **c)** Contributions of individual residues to the gating charge in second S4 step. (*Left* Y axis) and cumulative sums of gating charge contributions (Right Y axis and shown in a *blue line*) converge to the total gating charge of ~0.7 $e_0$ transferred for S4 intermediate to S4 in movement (Step 2). **d)** Molecular illustration of side chains contributing more that 10 % to the total gating charge movement in the second S4 step. S4 in structure shows side chains contributing positively to net gating charge transfer shown with transparent blue spheres. The radius of the sphere reflects relative contribution of the residue to gating charge moved in Step 2. In the kinetic model (Suppl. Fig. S5d), the first step is assumed to be independent in the four subunit and was best fit a $z = 2 \bullet 0.47\ e_0 = 0.94\ e_0$. In kinetic model, the second step is assumed to be cooperative in the four subunit and was best fit with $z_{coop} = 2 \bullet 1.5\ e_0 = 3.0\ e_0$. This is equivalent to a z per subunit of $z = z_{coop}/4 = 3.0/4 = 0.75\ e_0$.

**Supplementary Table S1. Summary of parameters of the fits for SPIH mutant channels**. $G_{1/2}$ and $F_{1/2}$ were obtained by fitting the G(V) and F(V) curves with a single Boltzmann equation. Data are shown as mean ± SEM. N indicates the number of replicates of all experiments.

| | $G_{1/2}$ | n | $F_{1/2}$ | n |
|---|---|---|---|---|
| wt* | -75.83 ± 0.48 | 3 | -54.70 ± 1.07 | 3 |
| E356A* | -96.28 ± 0.77 | 5 | 10.73 ± 2.08 | 4 |
| N370A* | -24.77 ± 1.03 | 3 | -21.99 ± 1.59 | 3 |
| E356A-N370A* | -42.56 ± 2.91 | 3 | -12.83 ± 1.16 | 4 |
| E356N* | -76.40 ± 1.71 | 4 | -33.06 ±1.68 | 4 |
| N370E* | -89.20 ± 1.40 | 3 | -63.63 ± 0.80 | 3 |
| E356N-N370E* | -56.84 ± 3.55 | 8 | -37.03 ± 0.60 | 4 |
| L340C-E356A* | -110.83 ± 2.44 | 3 | 31.20 ± 1.44 | 3 |
| E356Q* | -105.05 ± 1.01 | 3 | -63.38 ± 3.33 | 4 |
| N370D* | -111.82 ± 6.38 | 4 | -42.63 ± 1.91 | 6 |

**Supplementary Table S2. Parameters used for simulations in Supplementary Figures S5 and S6.**

| | wt* | E356A* |
|---|---|---|
| $k_1$ | 37.8 $s^{-1}$ | 117 $s^{-1}$ |
| $V_{1/2}(1)$ | -66.9 mV | 13.8 mV |
| $z_1$ | 0.47 $e_0$ | 0.47 $e_0$ |
| $k_2$ | 3.3 $s^{-1}$ | 2.7 $s^{-1}$ |
| $V_{1/2}(2)$ | -67.4 mV | -97.9 mV |
| $z_2$ | 1.50 $e_0$ | 1.50 $e_0$ |
| $\gamma_0$ | 0.89 $s^{-1}$ | 0.63 $s^{-1}$ |
| $\delta_0$ | 160 $s^{-1}$ | 137 $s^{-1}$ |
| $L_1$ | 1.67 | 1.14 |
| $L_2$ | 68.3 | 69.8 |
| $\Delta F_1$ | 0.25 | 0.25 |
| $\Delta F_2$ | -0.05 | -0.05 |

**Supplementary Video**

**Video S1. Two-step S4 movement during HCN channel opening.** We propose that the first S4 step in spHCN channels in response to a hyperpolarization is a helical-screw movement of S4 between two closed states with S4 outward and S4 inward. The second S4 step is a bending of S4 at residue S346. We propose that channel opening is favored by this bending of S4. The closed state spHCN model with S4 outward was modelled after the cryo-EM structure of the closed hHCN1 with S4 outward [1]. The open state spHCN model with S4 inward was modelled after the cryo-EM structure of the open hERG channel [3] with the VSD replaced for the hHCN1 VSD with S4 inward [2]. The closed state spHCN model with S4 in the intermediate state was modelled after the cryo-EM structure of the closed hHCN1 with S4 inward [2], but the VSD was remodeled to approximate the conformation of S1-S4 as in the S4 outward state [1]. However, N-terminal part of

S4 remained in the same vertical position as in the S4 inward state. The S4 helix was also straightened by rotating the C-terminal part of S4 to be more aligned with the N-terminal part of S4. Morphs between the two closed and one open HCN models suggest that the transition from closed to open involves first an inward helical-screw movement of S4 that breaks interactions that stabilize the S4 outward state, such as the E356-N370 hydrogen bond. This first S4 step is followed by a tilting of lower S4, which leads to a radial translation of lower S5 and S6 that opens the pore. In the open state with S4 inward, there is a large aqueous crevice around S4 and nearby residues, such as N370 and L340C. S4 residues R332, K335, S338, R341, R344, R347, and R350 are shown as stick. Only a single subunit is shown for clarity.

**Supplementary Data Sets S1**

Data Set for Fig. 1g. Normalized G(V) and F(V) curves of wt*, E356A*, N370A* and E356A-N370A* channels.
Data Set for Fig. 2b. Normalized G(V), F(V), and second component of the F(V) curves of E356A* channels.
Data Set for Fig. 2d. Exponential time constants of the ionic currents (I) and the first (F1) and second (F2) fluorescence component for E356A* and the gating currents (Q) for E356A-P435Y*.
Data Set for Fig. 3b. Normalized G(V) and F(V) curves of wt*, E356N*, N370E*, and E356N-N370E* channels.
Data Set for Fig. 4c. Normalized G(V) and F(V) curves of wt*and L340C-E356A* channels.
Data Set for Fig. 4g. Currents measured at the arrow in 4e and 4f from L340C-E356A channels during MTSET application at -40 mV and -100 mV.
Data Set for Fig. S2c. On and Off QV curves generated by integrating the currents in a and b from a representative oocyte.
Data Set for Fig. S3c. Normalized G(V) and F(V) curves of wt*, E356Q*, and N370D* channels.
Data Set for Fig S4d. Currents measured at the arrow in S4b and S4c from E356A-N370C channels during MTSET application at -40 mV and -100 mV.

**SI References**


1 Lee, C. H. & MacKinnon, R. Structures of the Human HCN1 Hyperpolarization-Activated Channel. *Cell* **168**, 111-120 e111, doi:10.1016/j.cell.2016.12.023 (2017).
2 Lee, C. H. & MacKinnon, R. Voltage sensor movements during hyperpolarization in the HCN channel. *Cell* **179**, 1582-1589.e1587, doi:10.1016/j.cell.2019.11.006 (2019).
3 Wang, W. & MacKinnon, R. Cryo-EM structure of the open human ether-a-go-go-related K+ channel hERG. *Cell* **169**, 422-430.e410, doi:10.1016/j.cell.2017.03.048 (2017).